Acceleration Challenge from 0 to 60,000 r/min in 1DOF Single-Drive Bearingless Motor with Pure Magnetic Suspension

Hiroya SUGIMOTO*, Naoki KAWASAKI*, and Yuki TANAKA*
*Department of Electrical and Electronic Engineering, Tokyo Denki University, Japan
E-mail: hiroya_sugimoto@mail.dendai.ac.jp

Abstract
One degree-of-freedom actively positioned bearingless motors and magnetic bearing motors have been studied to reduce costs and simplify the regulation system by reducing active positioning axes. Only axial direction of the rotor shaft is actively positioned, and the other axes of radial and tilting directions are passively stabilized with passive magnetic bearings. It has critical speeds that depend on the passive stiffness, and high acceleration is required to pass through the critical speed. This paper verifies the acceleration requirement in the experiment. In addition, this paper presents an adjustment method of a coefficient of time-delay compensation to reduce d-axis current that controls active axial forces. It is a key parameter to accelerate the bearingless motor up to 60,000 r/min with stable magnetic suspension. In the experiment, it is validated that the estimated optimal coefficient succeeds non-contact stable operations from the acceleration to the steady-state at 60,000 r/min.

Keywords : Bearingless Motor, One degree-of-freedom, Single-drive, Passive magnetic bearing, High-speed, Acceleration, Time delay compensation

1. Introduction

One of the most remarkable research topics is reducing active positioning axes in bearingless motors. One-axis actively positioned bearingless motors have been studied because their advantages are simple system and low cost [1]. In particular, single-drive bearingless motors are cost-effective because only one three-phase inverter and one displacement sensor are required for generating torque and axial suspension force [2]. These force and torque are actively regulated by q- and d-axis currents, respectively. Therefore, the regulation system is rather simple compared to other bearingless motors that have two or much degrees of freedom.

On the other hand, shaft vibrations have been the most significant issue. One degree-of-freedom (1DOF) actively positioned bearingless motors passively stabilize the radial and tilting motions so that their vibrations increase around a critical speed. In fact, it is reported that the radial and tilting vibrations are significantly high at critical speeds in [3]-[7]. In [5], a viscoelastic material is installed between the stator and the base so that damping forces reduce the radial and tilting vibrations. In [6], the resonant vibration is reduced by shifting the stator permanent magnet using a linear actuator. In [7], radial and tilting vibrations are reduced at the critical speed by high motor accelerations. As a result, the rotor shaft passes through critical speed without touch-down. These vibration reduction techniques are significantly effective for improving rotor rotational speeds.

In [8], a single-drive bearingless motor achieves an acceleration up to 20,000 r/min. Although the maximum speed is 30,000 r/min, it does not achieve acceleration of 0 – 30,000 r/min because axial vibrations are increased in high-speed region. It is caused by a coupling between d- and q-axis current regulation systems. There is another cause of time-delay in the digital control system. In case of single-drive bearingless motors, both the coupling and the time-delay are serious problems for magnetic suspension. In [9], the stator core material and the number of turns are improved from the aforementioned single-drive bearingless motor. The improved prototype machine achieves acceleration from 0 – 30,000 r/min with both the time delay compensation and the decoupling control between dq axes. In [10], a 60,000 r/min slotless single-drive bearingless motor is proposed. It has aerodynamic bearings to stabilize the radial and tilting directions. The axial direction of the rotor shaft is also passively stabilized due to the magnetic pull between the rotor permanent magnet

and the stator back core.

This paper presents a challenge of increasing the rotational speed up to 60,000 r/min in the single-drive bearingless motor with pure magnetic suspension. The prototype machine does not have any other bearings except magnetic suspensions. Firstly, the q-axis requirement to pass through critical speeds is verified in acceleration tests. Secondly, a coefficient of the time-delay compensation is a key parameter for stable magnetic suspension. It is optimized to minimize d-axis current that is used to control the rotor axial position. Finally, in the acceleration test, it is demonstrated that the prototype machine successfully achieves 60,000 r/min with stable magnetic suspensions.

2. Prototype Machine of 1DOF Single-Drive Bearingless Motor

Figure 1 shows a cut view of the one-axis actively positioned single-drive bearingless motor [9]. It has two sets of repulsive passive magnetic bearings at both ends of the rotor shaft. Two-layer four-pole rotor permanent magnets generate rotating torques and active axial forces. These torque and force are regulated by q- and d-axis currents, respectively, in the one set of three-phase winding that is wound in the center stator core. This single-drive bearingless motor topology has great advantages of reducing numbers of inverters and displacement sensors. In fact, it requires only one three-phase inverter and one displacement sensor. The rotor has carbon fiver bandages that are covered with rotor permanent magnets. The rotor PMBs are also coved with the bandage. The physical gap is approximately 2 mm between the rotor cover and the stator permanent magnet. The stator outer diameter and the axial length are 64 mm and 40.4 mm, respectively, and the rated power is approximately 60 W at 60,000 r/min.

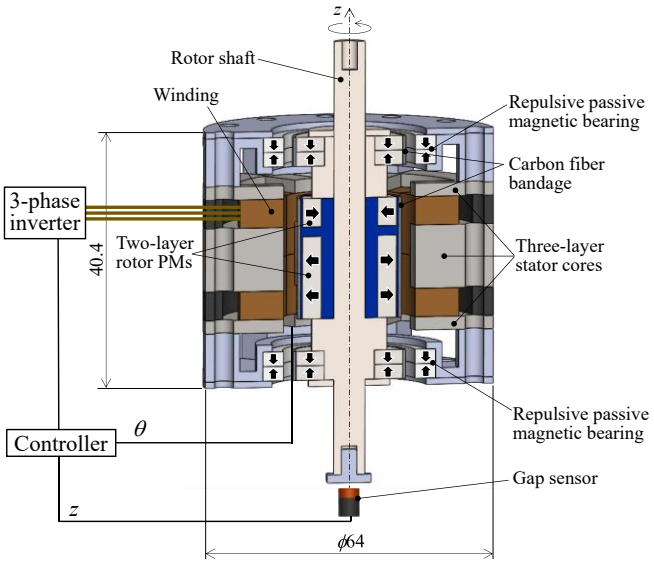

Fig. 1. Cut view of 1DOF single-drive bearingless motor.

Table 1 shows parameters in the prototype machine of the 1DOF single-drive bearingless motor. The rotor outer diameter and the shaft length are 18 mm and 69.7 mm, respectively. Then, the mass and the inertia around z-axis are 0.0498 kg and 1.45×10^{-6} kg·m, respectively. There are two mechanical gaps at the passive magnetic bearing and the single-drive bearingless motor parts, and they are 1.5 mm and 2.2 mm, respectively. The mechanical gap is relatively large to avoid touchdowns at critical speeds. Even when the mechanical gap is large enough, the rotor shaft would be touchdown on the stator because the radial vibration is inherently infinite at the critical speed. Therefore, the acceleration should be improved to pass through the critical speed before the vibration is amplified.

Table 1 Parameters in prototype machine

Parameter	Symbol	Value	Unit
Stator outer diameter	D_s	46.0	mm
Stator axial length	l_s	40.4	mm
Rotor outer diameter	D_r	18.0	mm
Shaft length	l_r	69.7	mm
Rotor mass	m	0.0498	kg
Magnetic gap at RPMB part	g_{mag_RPMB}	2.0	mm
Mechanical gap at RPMB part	g_{mec_RPMB}	1.5	mm
Magnetic gap at SDBM part	g_{mag_SDBM}	3.0	mm
Mechanical gap at SDBM part	g_{mec_SDBM}	2.2	mm
Number of turns per tooth	-	46	turn
Winding wire diameter	D_w	0.5	mm
DC resistance of winding per phase	R	0.321	Ω
Phase inductance	L	0.236	mH
Inertia around x- and y-axis	J_r	1.11×10^{-5}	kg·m
Inertia around z-axis	J_z	1.45×10^{-6}	kg·m

Figures 2(a) and 2(b) show principles of torque and active axial force generations, respectively. The xy cross section shows a four-pole/six-slot surface permanent magnet machine. The stator core has four-pole three-phase concentrated windings, and it generates magnet torques by q-axis current. In Fig. 2(b), the solid black arrows indicate the magnetization directions of the two-layer four-pole rotor permanent magnets. The black broken arrows indicate the permanent magnet fluxes. They go to stator teeth through air gaps, and circulate radially in stator yokes. The red arrows indicate d-axis fluxes that are generated by the stator winding, and these fluxes circulate in the axial directions between the center stator and upper/lower stator cores in each air-gap. As a result, the active axial force is generated by unbalanced

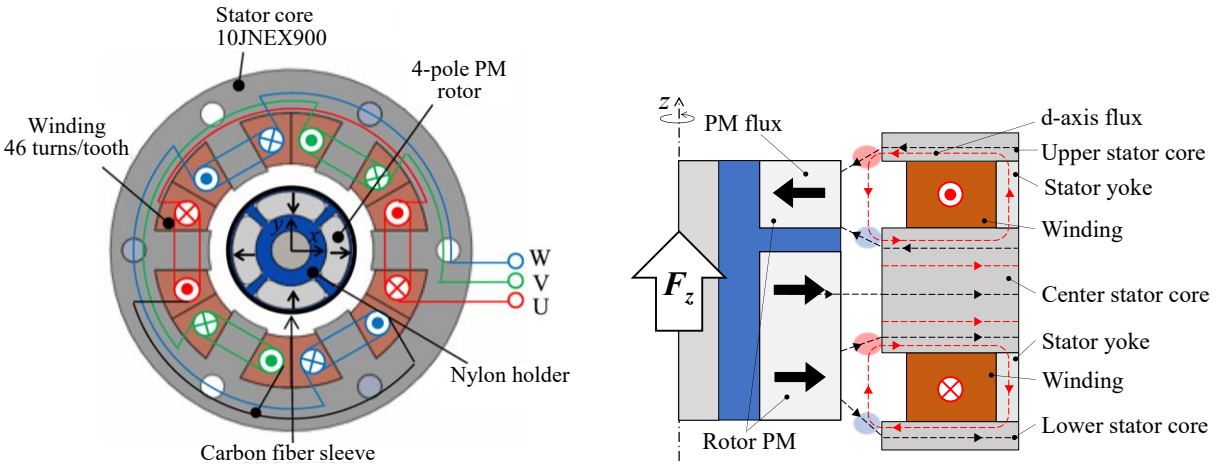

(a) xy-cross sectional view (b) xz-cross sectional view

Fig. 2. Principles of torque and active axial force generations in 1DOF single-drive bearingless motor.

flux density distributions in air gaps. Therefore, the active axial force can be regulated by d-axis current. In addition, d-axis fluxes circulate in the radial direction as shown in straight red arrows in the center stator core. The flux-strengthening increases the unbalanced magnetic pull, and it decreases passive radial stiffness. On the other hand, the flux-weakening generates axial forces in the negative axial direction, and it reduces the unbalanced radial force so that the passive radial stiffness is enhanced.

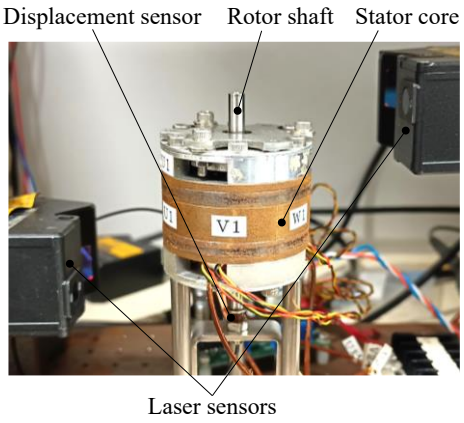

Fig. 3. Prototype machine of single-drive bearingless motor.

Figure 3 shows the prototype machine of the single-drive bearingless motor. The radial and tilting directions are passively stabilized with repulsive passive magnetic bearings. Only axial direction is actively positioned. This prototype machine is pure magnetic suspension system because it does not have any other bearings such as aerodynamic bearings, hydrodynamic bearings, and oil film bearings. The axial position of the rotor shaft is measured by the displacement sensor that is installed under the shaft as shown in Fig. 3. Two laser sensors are installed to monitor the shaft vibration.

3. Regulation System for High-Speed 1DOF Single-Drive Bearingless Motors with Decoupling Control in between dq Axes and Time-Delay Compensation

Figure 4 shows the proposed control block diagram of single drive bearingless motor. The d-axis current reference i_d^* is generated from the Proportional-Integral-Derivative (PID) controller based on detected rotor axial position z by a displacement sensor. The q-axis current reference i_q^* is generated from the Proportional-Integral (PI) controller based on

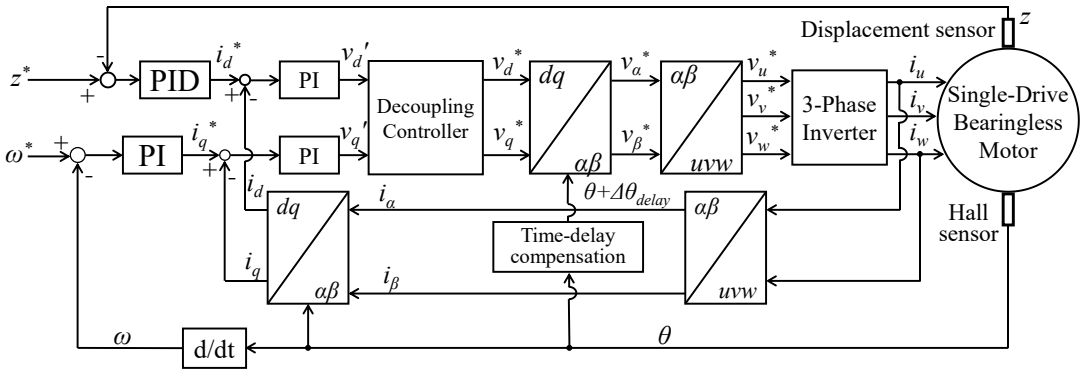

Fig. 4. Regulation system of single-drive bearingless motor.

calculated rotational speed ω. The rotational speed is calculated by differentiated the angle detected by six hall sensors. Then, d- and q-axis voltage references are generated via current PI controllers. In the previous controller in [8], their voltage references include coupling terms so that the rotor axial vibration are considerable high during the acceleration. In the measured waveforms of d- and q-axis currents, we can see serious current ripples at high-speed region. In this paper, let us apply a general decoupling controller for reducing current ripples. Let us define d- and q-axis inductances L_d and L_q, the electrical angular frequency ω_e, and a coefficient of back EMFs K_E. In addition, previous and corrected voltage references are defined as v_d', v_q', and v_d^*, v_q^*, respectively, as shown in Fig. 4. These voltage reference v_d^* and v_q^* are given as follows:

$$v_d^* = v_d' - \omega_e L_q i_q , \tag{1}$$

$$v_q^* = v_q' + \omega_e L_d i_d + K_E \omega_e . \tag{2}$$

The d-axis voltage reference is corrected by subtracting the induced voltage due to q-axis current. It is significantly effective for reducing the coupling of q-axis current that is instantaneously increased in the motor acceleration. The rotor axial vibration can be reduced by (1). The q-axis voltage reference is also corrected by (2). These corrections are necessary for stable magnetic suspensions in accelerations and high-speed drives.

In Fig. 4, a time-delay compensation block is included because the digital control system has the time-delay caused by a sampling time. When the sampling period is defined as T_s, the time-delay $\Delta\theta_{delay}$ is given as follows:

$$\Delta\theta_{delay} = k_{td}\omega_e T_s . \tag{3}$$

It is also one of the serious problems in high-speed region because it increases error angles, and in the worst case, the rotor shaft would be touch-down. As can be seen in Fig. 4, the detected angular position θ is corrected by adding the time-delay $\Delta\theta_{delay}$. Generally, the time-delay $\Delta\theta_{delay}$ is approximately one-and-a-half sampling period so that the coefficient is k_{td} = 1.5 [11]. On the other hand, it should be increased more than 1.5 to achieve high-speed operation.

4. Acceleration Tests and Optimal Coefficient of Time-Delay Compensation toward 60,000 r/min

Figure 5 shows measured acceleration waveforms to investigate the requirement of q-axis current to pass through the critical speed. The q-axis current is changed from 0.5 A to 3 A for increasing the acceleration of the bearingless motor. As can be seen in Fig. 5, low accelerations at i_q = 0.5 A and 1 A do not reach the target rotation speed of 30,000 r/min because the rotor shaft is touchdown the stator. On the other hand, it reaches 30,000 r/min over i_q = 1.5 A, and the acceleration requirement is 49,302 (r/min)/s that is calculated from a rate of change from 5,000 to 10,000 r/min. The acceleration is proportional to the q-axis current, and the torque is approximately estimated from the acceleration as follows:

$$T = \frac{2\pi J_z}{60}\frac{dN_m}{dt} . \tag{4}$$

Note that both windage and eddy current losses are ignored because of large mechanical gaps and no-load condition.

Figure 6 shows the estimated torques form the rate of change of the acceleration. These plots are mostly aligned on a torque curve calculated in three-dimensional finite-element-method (3D-FEM) analysis. The toque constant is 5.1 mNm/A so that

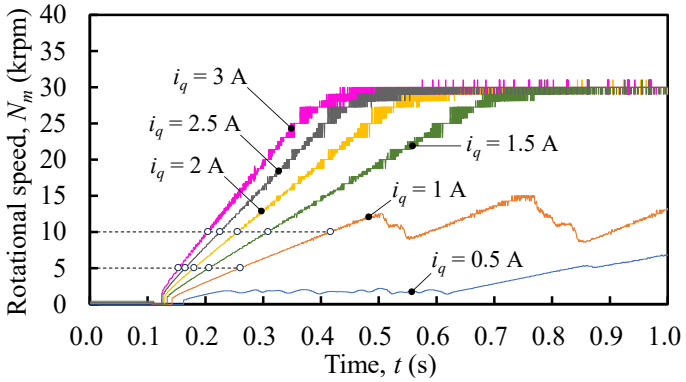

Fig. 5. Measured acceleration waveforms when q-axis current is changed.

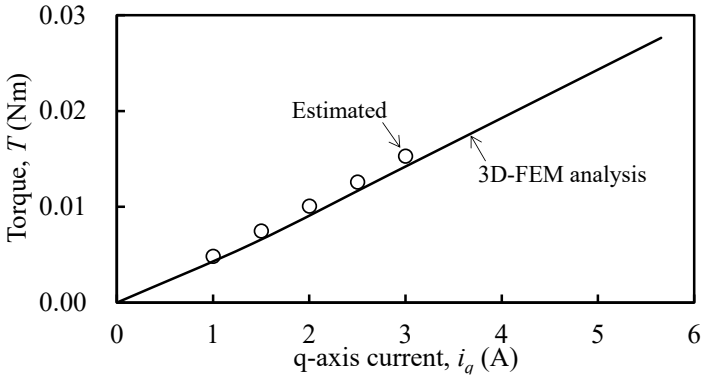

Fig. 6. Calculated and estimated torques.

the torque requirement for passing through the critical speed is 7.5 mNm at i_q = 1.5 A.

Figure 7 shows an influence of the coefficient of the time-delay compensation. The d-axis current mainly includes four harmonic components. The mechanical and electrical fundamental components are 500 Hz and 1,000 Hz, respectively, at 30,000 r/min. A sum of these components is reduced with an increase of the coefficient. On the other hand, third and fourth components are increased in the case high coefficient. As a result, the d-axis current is minimized with k_{td} = 1.65 when the rotational speed. This optimized coefficient is changed when the rotational speed is increased.

Figure 8 shows the optimized coefficient of the time-delay compensation with respect to the rotational speed. It is proportional to the speed, and then, the coefficient should be 2.05 at 60,000 r/min. The fundamental current frequency reaches 2 kHz at 60 kr/min. A sampling frequency in a digital controller is 20 kHz. Therefore, a sampling-to-fundamental (S2F) frequency ratio is equal to 10. This case is a low S2F frequency ratio, and it leads to instability of the drive system [12]. In fact, the d-axis current sensitively varies by changing the coefficient of the time-delay compensation. Thus, the coefficient should be carefully chosen in the case of low S2F ratio.

Figure 9 shows measured acceleration waveforms of the rotational speed, q-axis current, d-axis current, and the axial position. The maximum q-axis current is set to 2 A that is good enough for passing through the critical speed as shown in Fig. 5. The rotor shaft is already levitated before the acceleration. The coefficient of the time-delay compensation is changed to 2.05. After that, the acceleration starts at 1 s, and the rotational speed reaches 60,000 r/min at approximately 2 s. The q-axis current is converged to 0 A at the steady-state because of no-load test. Axial vibrations occur during the acceleration, and then, it is suppressed at the steady-state. The d-axis current is increased to suppress the axial vibration at the acceleration, and it is still needed to stabilize the axial position at the steady-state. In this acceleration test, the prototype single-drive bearingless motor achieves the stable acceleration up to 60,000 r/min with the optimized coefficient of the time-delay compensation.

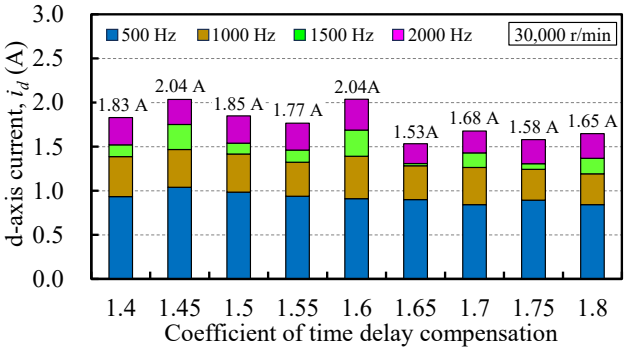

Fig. 7. d-axis current with respect to coefficient of time-delay compensation.

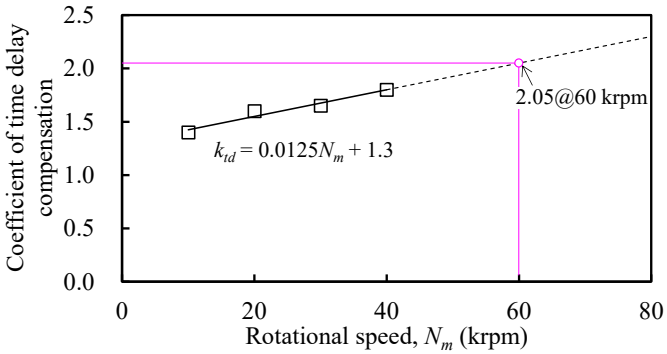

Fig. 8. Optimized coefficient of time-delay compensation with respect to rotational speed.

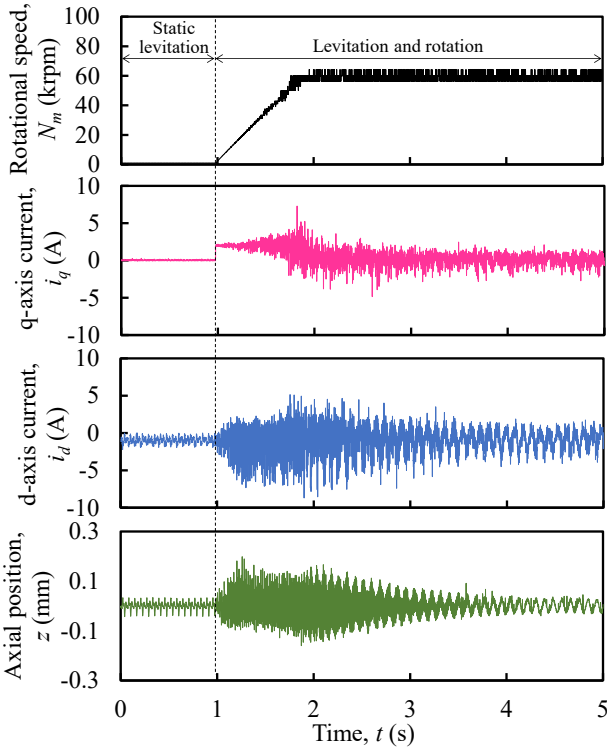

Fig. 9. Measured waveforms during acceleration up to 60,000 r/min.

5. Conclusions

This paper shows a unique test result of the rotor acceleration up to 60,000 r/min in the 1DOF single-drive bearingless motor with pure magnetic suspension. The prototype machine passes through critical speeds with a reasonable q-axis current of i_q = 1.5 A. The coefficient of the time-delay compensation is optimized, and it is proportional to the rotational

speed. It should be increased more than 1.5 which is frequently used value, and as a result, it is 2.05 at 60,000 r/min. In the acceleration test, the prototype machine successfully demonstrates the acceleration up to 60,000 r/min with the optimal coefficient. This achievement makes a valuable knowledge of 1DOF single-drive bearingless motors that can increase the rotational speed even when the low sampling-to-fundamental frequency ratio.

6. Acknowledgments

This work was supported by JSPS KAKENHI Grant Number 23K26062, 24K00875. The authors would like to thank Mr. Minoru Watanabe of Tokyo Denki University for his contribution.

References

W. Bauer et al., “Electrical Design Considerations for a Bearingless Axial-Force/Torque Motor”, in *IEEE Trans. Ind. Appl*., vol. 50, no. 4, pp. 2512–2522, 2014.

J. Asama et al., “Proposal and Analysis of a Single-Drive Bearingless Motor", *IEEE Trans. Ind. Electron.*, vol. 60, no. 1, pp. 129-138, 2013.

T. Ohji et al., “Structure of One-Axis Controlled Repulsive Type Magnetic Bearing System With Surface Permanent Magnets Installed and Its Levitation and Rotation Tests,” *IEEE Transactions on Magnetics*, vol. 47, no. 12, pp. 4734-4739, 2011.

J. Asama et al., “Development of a One-Axis Actively Regulated Bearingless Motor with a Repulsive Type Passive Magnetic Bearing", *in Proc. IPEC-Hiroshima 2014-ECCE-Asia*, pp. 988-993, 2014.

J. Passenbrunner et al., “Simulation and Optimization of an Active Axial Bearing with Viscoelastic Damping Support,” *in Proc. IEMDC2017*, pp. 1-6, 2017.

T. Inoue et al., “Vibration suppression of the rotating shaft using the axial control of the repulsive magnetic bearing,” *J. Syst. Des. Dyn.*, vol. 4, no. 4, pp. 575–589, 2010.

H. Sugimoto et al., “Dynamic Modeling and Experimental Validations of Passing Through Critical Speeds by High Acceleration in One-Axis Actively Positioned Bearingless Motors,” in *IEEE Trans. Ind. Appl.*, vol. 57, no. 6, pp. 6956-6964, 2021.

T. Srichiangsa et al., “Design, Development, and Experimental Results of a 30 000-R/Min One-Axis Actively Positioned Single-Drive Bearingless Motor,” in *IEEE Trans. Ind. Appl.*, vol. 57, no. 6, pp. 6783-6791, 2021.

H. Sugimoto et al., "Variable Passive Radial Stiffness in Single-Drive Bearingless Motors for Changing Rotor Natural Frequency," *in Proc., IEMDC2023*, pp. 1-6, 2023.

J. Asama, "Development of Slotless Single-Drive Bearingless Permanent Magnet Motor With Aerostatic Bearings for High-Speed Applications," in *IEEE Trans. Ind. Appl.*, vol. 59, no. 4, pp. 4076-4082, 2023.

Bon-Ho Bae et al., "A compensation method for time delay of full-digital synchronous frame current regulator of PWM AC drives," in *IEEE Transactions on Industry Applications*, vol. 39, no. 3, pp. 802-810, 2003.

M. Wang et al., "Decoupled Discrete Current Control for AC Drives at Low Sampling-to-Fundamental Frequency Ratios," in *IEEE Journal of Emerging and Selected Topics in Power Electronics*, vol. 11, no. 2, pp. 1358-1369, 2023.